Catalysis Today 384-386 (2022) 166–176

Contents lists available at ScienceDirect

Catalysis Today

journal homepage: www.elsevier.com/locate/cattod

AgAu nanoclusters supported on zeolites: Structural dynamics during CO oxidation

I. López-Hernández [a], V. Truttmann [b], C. Garcia [b], C.W. Lopes [c], C. Rameshan [b], M. Stöger-Pollach [d], N. Barrabés [b,*], G. Rupprechter [b], F. Rey [a], A.E. Palomares [a,*]

[a] Instituto de Tecnología Química, Universitat Politècnica de València - Consejo Superior de Investigaciones Científicas (UPV-CSIC), Valencia, Spain
[b] Institute of Materials Chemistry, TU Wien, Vienna, Austria
[c] Institute of Chemistry, Universidade Federal do Rio Grande do Sul, Porto Alegre, Brazil
[d] University Service Center for Transmission Electron Microscopy (USTEM), Technische Universität Wien, Wiedner Hauptstraße 8-10, 1040, Vienna, Austria

ARTICLE INFO

Keywords:
CO oxidation
Metal nanoclusters
Doping
Silver
Gold
Zeolites

ABSTRACT

The bimetallic nanocluster catalyst structure can change during pretreatment and reaction, thus *in situ* characterization techniques are required for a proper analysis of the active sites. *In situ* XAFS and DRIFTS were used to study the dynamic evolution of the metal active sites in bimetallic Ag_xAu_{25-x} nanoclusters supported on ITQ2 zeolite during CO catalytic oxidation. The activity of the bimetallic nanocluster catalyst in this reaction was significantly higher than those of supported monometallic Ag_{25} and Au_{25} nanoclusters. These results were explained by the formation of AgAu alloyed nanoparticles, which favoured reactant adsorption and reaction. Furthermore, the initial activity depended on the catalyst pretreatment, obtaining better conversion, at lower temperatures, with the catalyst pretreated with hydrogen than with the catalyst pretreated with oxygen. This was also associated with an easier formation of a AgAu alloy under hydrogen pretreatment at 150 °C. However, the alloying process seemed to be completed after reaction in both cases, *i.e.* for the catalyst pretreated with oxygen and with hydrogen, obtaining the same catalytic performance with both catalysts upon reuse. The activity is constant in successive reaction runs, indicating high stability of the active species formed under reaction conditions. The results have shown that the combination of catalytic studies with *in situ* characterization techniques provides insight into the structural dynamics of the catalysts during activation and reaction.

1. Introduction

The development of nanoscience and the versatile chemistry of metal nanoparticles have led to a substantial increase in the use of these materials for heterogeneous catalysis [1,2]. Supported metal nanoparticles and nanoclusters have been used as efficient catalysts in both oxidation and hydrogenation reactions [1,3,4]. Among them, gold nanoparticles are a special subject of interest due to their optical [5] and catalytic properties [1,6–8]. Haruta et al. [9] first described that supported gold nanoparticles catalysts can achieve noteworthy activity in CO oxidation even at temperatures as low as -70 °C. Silver nanoparticles, similarly, showed significant activity for CO oxidation that depended on the particle size [10]. Nevertheless, the stability of these catalysts is still a problem to be solved [11].

Many researchers have investigated the synthesis of stable metal nanoclusters with well-defined structures. In particular, thiolate-protected gold nanoclusters ($Au_n(SR)_m$) have demonstrated to be materials with exceptional catalytic activity [4,12–14]. In general, the activity of supported nanoparticles and nanoclusters depends strongly on different factors such as metallic valence state [15,16], the nanoparticle/nanocluster size [3,17–21], the pretreatment conditions [22], the ligands [23], and the support used [6,19,24]. In previous studies, a different stability and reactivity of the cluster catalysts, depending on the material used as support [12,13,19,22,25,26], was observed. Reducible oxides as CeO_2 and TiO_2 led to strong interaction with the metal nanoclusters, not only stabilizing them, but also affecting their catalytic performance. Contrary, in the case of SiO_2, stabilization of the clusters without further effect was obtained [19].

Among the different supports used for metallic nanoparticles, the structure of zeolites leads to the formation of unique clusters and electronic states. This is due to their high surface area as well as their possible ionic exchange properties, special morphology and different

* Corresponding authors.
E-mail addresses: noelia.rabanal@tuwien.ac.at (N. Barrabés), apalomar@iqn.upv.es (A.E. Palomares).

https://doi.org/10.1016/j.cattod.2021.04.016
Received 23 November 2020; Received in revised form 16 February 2021; Accepted 16 April 2021
Available online 19 April 2021

chemical composition. These factors can be selectively fine-tuned [27–30], thereby obtaining optimized supports for each specific use. In a previous paper [31], we have shown that depending on how silver is incorporated into a laminar zeolite, diverse sites are formed with different activity for the CO oxidation reaction.

The metal nanoclusters' properties and therefore the catalytic activity can be also altered by doping with other metals [4,32]. The replacement of the central atom of Au_{25} by 16 different metals has been reported [33]. Tsukuda et al. described that a Ag atom doped in a Au_{25} structure did not occupy the central position, but a surface site in the Au_{13} core instead. This leaded to a very stable structure, as confirmed by X-ray absorption spectroscopy combined with DFT calculations [34].

Even though silver and gold both have an fcc bulk-metallic structure with a similar atomic size, their physicochemical properties are quite different. As a consequence, replacing Au atoms in a gold nanocluster by Ag can modify their electronic structure [35] leading to changes in the optical absorption spectra [36], as well as in the luminescence behaviour [37,38]. Moreover, Ag doping can also induce enhanced structural flexibility [39] and chirality [40]. Consequently, it can be expected that AgAu nanostructures are interesting for several applications [41,42] as they can lead to increased reactivity while assuring structural stability.

CO oxidation is a widely studied catalytic reaction involving nanomaterials [6,7]. It is usually employed to remove this pollutant that is produced during incomplete combustion processes in vehicles and industries. It can be also used as a test reaction to investigate the nanoparticle properties [31,43] that depend on the cluster structure [20], support material [44–46] and thermal pretreatment. The latter has been related to the partial removal of the protecting ligand sphere, enhancing the nanocluster reactivity [13,47].

The nanocluster doping effect can be also studied by the CO oxidation reaction. It was reported that for CeO_2-supported doped gold nanoclusters the activity in this reaction has the tendency Cu_x-$Au_{25-x}(SR)_{18} > Au_{25}(SR)_{18} > Ag_xAu_{25-x}(SR)_{18}$ [48]. Other authors [49,50] found that the Ag-Au sites were more favourable adsorption sites compared to the monometallic sites by DFT calculations. They further showed that a reductive pretreatment fostered an increase of the silver content on the surface [49]. The mobile nature of dopant atoms in heterogeneous nanoclusters has also been reported in our previous work on PdAu nanoclusters on TiO_2, where the combination of oxidative and reductive pretreatment, as well as the reaction, led to migration of Pd to the surface. Thereby, the creation of accessible Pd single sites resulted in a significant increase in activity compared to Au_{25}/TiO_2 [25].

These examples clearly show that certain nanocluster properties are prone to change during catalyst pretreatment and/or reaction, thus resulting in different catalytic performances. Unraveling the nature of these changes and understanding how they affect the reactivity is of utmost importance in catalysis research since it could aid the development of new highly active and stable catalytic materials.

Within this work, we used catalytic CO oxidation together with a combined analysis of *in situ* DRIFTS and EXAFS measurements to study the nature and evolution of the metallic sites in silver-gold nanoclusters supported on pure silica ITQ2 zeolite. The pure silica zeolite belongs to the same group of SiO_2 or MgO supports, which are less active at low temperatures in comparison to the reducible oxide supports [51–53], therefore, using ITQ2 as support will allow better understanding of clusters' catalytic activity. The characterization studies have been related to the catalytic results, thus determining which metallic site properties are relevant for catalyst activity.

2. Experimental

2.1. Catalyst preparation

Pure silica ITQ2 delaminated zeolite was used as support, which was prepared according to [54]. $Au_{25}(SC_2H_4Ph)_{18}$ nanoclusters and $Ag_{25}(SPhMe_3)_{18}PPh_4$ nanoclusters were synthesized according to [55] and [56], respectively. $Ag_xAu_{25-x}(SC_2H_4Ph)_{18}$ clusters were synthesized and characterized by the procedure described in the Supporting Information.

In order to support the nanoclusters on the zeolite, the necessary amount of each nanocluster to obtain a 1 wt.% metal loading was dissolved in toluene and stirred together with the ITQ2 zeolite for 24 h at room temperature. After that, the sample was centrifuged and separated from the solution by decantation. Then, the catalyst was dried at 80 °C for 1 h.

2.2. Pretreatment

Different pretreatments (oxidative and reductive) were applied before the catalytic tests to study their effect on the nanocluster structure and therefore on the catalytic activity. Both pretreatments were made at 150 °C (10 °C min^{-1} heating ramp, holding for 1 h). The oxidative pretreatment ($pretO_2$) was performed using 5% O_2 in nitrogen (with a total flow of 500 mL min^{-1}) and the reductive one ($pretH_2$) with the same total flow but containing 5% H_2 in nitrogen.

2.3. Catalytic tests

Catalytic CO oxidation was carried out at atmospheric pressure in a fixed-bed quartz reactor with 250 mg of sieved catalyst (0.4−0.6 mm). The total gas flow was 500 mL min^{-1} with 0.5 % CO, 4% O_2 and N_2 as balance gas with a space velocity of 318,000 h^{-1}. The reaction was performed from 100 °C to 500 °C, increasing by 50 °C in each step. The CO_2 concentration was continuously monitored with an infrared spectroscopy analyser of Servomex, Model 4900 with an accuracy of 0.01 %

2.4. In situ studies

Diffuse reflectance infrared Fourier transform spectroscopy (DRIFTS) studies were carried out on a Bruker Vertex 70 spectrometer with a liquid N_2-cooled MCT detector and with 4 cm^{-1} resolution. DRIFTS spectra were taken throughout the whole experiment by averaging 256 scans to achieve a good signal to noise ratio. The stainless-steel flow cell (Pike) has a CaF_2 window and an oven. The inlet of the cell was connected to a gas manifold system with calibrated mass flow controllers to adjust the gas mixtures and a mass spectrometer for kinetic measurements. Each sample was placed into a small ceramic cup and the exact weight was taken for normalization (~30 mg). The sample was pretreated as in the catalytic tests. Then, the gases were changed to reaction conditions without removing the sample in between. The reaction temperature was increased with a heating ramp of 5 °C min^{-1} to 400 °C and kept for 30 min. Afterwards, the sample was cooled to room temperature (under reaction gas atmosphere). Spectra measured after catalyst pretreatment were used for background removal.

X-ray Absorption Spectroscopy (XAS) study was performed at the CLAESS beamline at ALBA synchrotron. Measurements were made in fluorescence mode (Ag K-edge and Au-L_3 edge) in the beamline's solid/gas reactor multipurpose cell. The catalysts were pressed into pellets and the samples were pretreated inside the multipurpose cell at 150 °C for 30 min under oxygen or hydrogen flow ($pretO_2$: 5% O_2 in He, 45 mL min^{-1}; $pretH_2$: 5% H_2 in He, 45 mL min^{-1}. After cooling down, the gas mix was changed to reaction conditions (reaction: 1.7 % CO, 3.3 % O_2 in He, total flow: 45 mL min^{-1}). The samples were heated to 150 °C with a ramp of 5 °C min^{-1}, the temperature was held for 30 min (COox150), and then further heated till 400 °C (COox400). The maximum temperature was held for 30 min, and then the reaction chamber was cooled to RT (45 mL min^{-1} He). Extended X-ray Absorption Fine Structure (EXAFS) spectra were taken at 40 °C in He at the beginning, after pretreatment and after reaction for each sample, without opening the reaction chamber in between. Data reduction/normalization was performed with the Artemis package [57], which uses the FEFF6 code [58] for amplitude and phase calculations for

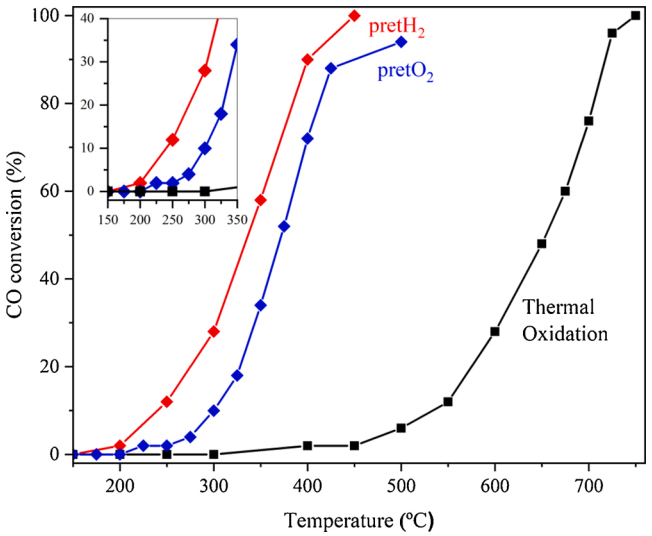

Fig. 1. Catalytic activity of the bimetallic Ag_xAu_{25-x}/ITQ2 in the CO oxidation reaction after oxidative ($pretO_2$) and reductive ($pretH_2$) pretreatments.

EXAFS fittings. Further details can be found as footnotes in the EXAFS tables.

2.5. Characterization studies

X-ray photoelectron spectroscopy (XPS) measurements were performed on an *in situ* NAP-XPS system equipped with a Phoibos 150 NAP hemispherical analyzer and a XR 50 MF X-ray source (microfocus), all SPECS GmbH. Spectra were recorded with monochromatic Al Kα radiation and data were analysed with the CasaXPS software. Peaks were fitted after linear background subtraction with Gauss – Lorentz sum functions. Peak positions and full width at half-maximum (FWHM) were left unconstrained. Au4f peaks were fitted with 3.7 eV doublet separation and a fixed ratio of 4:3 for $Au4f_{7/2}$ and $Au4f_{5/2}$. For the $Ag3d_{5/2}$ and $Ag3d_{3/2}$ peaks doublets with a fixed separation of 6 eV and a fixed area ratio of 3:2 were used (all NIST XPS database). For the NAP-XPS measurements the sample was applied evenly on carbon tape. The actual measurements were conducted at elevated pressure in 1 mbar inert gas (N_2) to avoid reduction of the clusters. Peak positions were referenced to the SiO_2 peak (both to Si2s and O1s component) which is the support material and gives the strongest signal [59].

Transmission electron microscopy (TEM) and high-angle annular dark-field scanning transmission electron microscopy (HAADF-STEM) was performed using a 200 kV FEI Tecnai F20 S-TWIN analytical (scanning) transmission electron microscopy [(S)TEM] instrument. Supported clusters were directly deposited on carbon-coated copper grids and plasma cleaning was applied to remove possible hydrocarbons and adsorbed water.

Temperature programmed reduction with H_2 analysis (H2-TPR) has been performed in a TPD-TPR Autochem 2910 equipment connected to a thermal conductivity detector (TCD). Prior to the reduction, samples were treated under Ar flow during 1 h at room temperature. During the TPR analysis, a mix of 10 % H_2 in Ar was used while the temperature was increased from room temperature to 600 °C with a ramp of 10 °C/min.

3. Results

Silver atoms were introduced to the Au_{25} nanoclusters and $Ag_xAu_{25-x}(SR)_{18}$ nanoclusters (simplified as Ag_xAu_{25-x}) were successfully obtained. The synthesized nanoclusters have a narrow distribution of Ag dopant atoms (x = 6–8, see Supporting Information). This was confirmed by matrix-assisted laser desorption-ionization mass spectrometry (MALDI-MS) and Ultraviolet-visible (UV–vis) spectroscopy (Supporting Information, Fig. S1). Besides the bimetallic nanoclusters, the monometallic Au_{25} and Ag_{25} nanoclusters were also prepared as it is referenced in Supporting Information. All nanoclusters were supported on pure silica delaminated zeolite (ITQ2). XRD and textural properties of the zeolite are shown in Supporting Information (Fig. S2).

3.1. Catalytic activity in CO oxidation

The catalytic application of the supported nanoclusters requires a pretreatment step to partially remove the ligand shell and to make the nanocluster metal surface accessible. Nevertheless, depending on the type of pretreatment, different modifications of the nanoclusters properties could occur [13,19,22,25,26]. Therefore, the effect of an oxidative ($pretO_2$) and a reductive ($pretH_2$) pretreatment on the catalyst activity

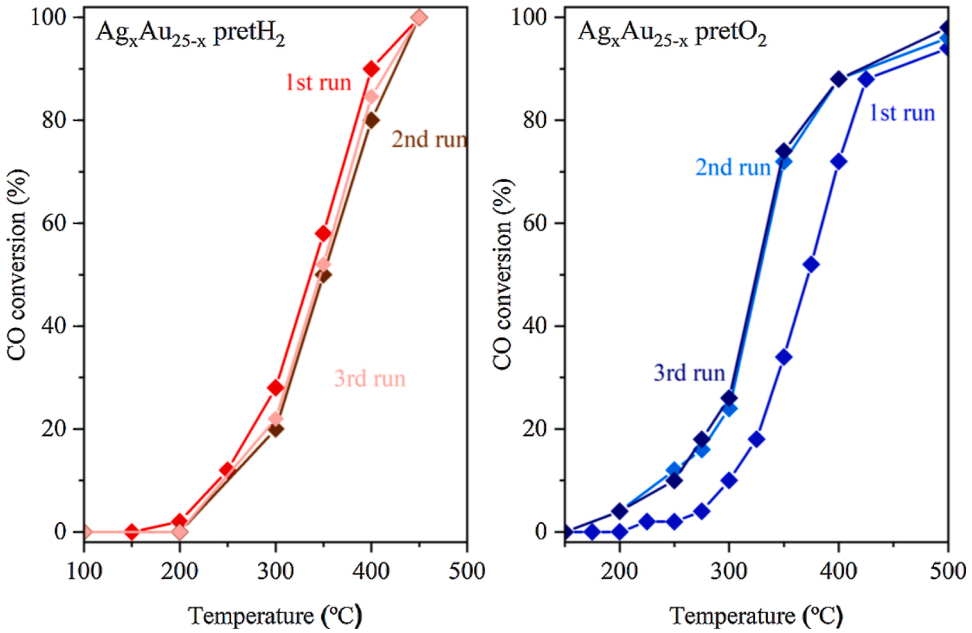

Fig. 2. CO oxidation activity of the bimetallic Ag_xAu_{25-x}/ITQ2 catalysts after different pretreatments in successive reaction cycles.

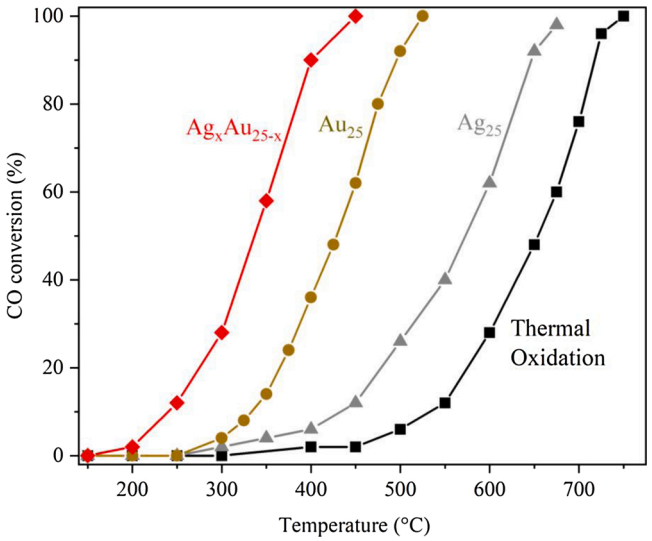

Fig. 3. Catalytic CO oxidation activity of mono- and bimetallic nanoclusters supported on ITQ2 after H_2 pretreatment.

was studied. Fig. 1 shows the results obtained for the CO catalytic oxidation reaction with the Ag_xAu_{25-x} bimetallic nanoclusters supported on the zeolite after both pretreatments.

The bimetallic nanoclusters supported on ITQ2 zeolite (Ag_xAu_{25-x}/ITQ2) were active catalysts for CO oxidation after both pretreatments, obtaining high conversion at much lower temperatures than those necessary for the uncatalyzed thermal reaction. The comparison of the different pretreatments showed that the catalyst pretreated with hydrogen was more active than the one pretreated with oxygen, with the differences being more pronounced at low temperatures. It can be observed that hydrogen pretreatment induced catalytic activity at 200 °C, whereas 250 °C are required for the catalyst pretreated with oxygen. These results already suggest a distinct evolution of the bimetallic nanocluster structure on the zeolite surface under the different pretreatments conditions. The possible activity of the support was also studied and as it can be seen in the Supporting Information (Fig. S3), the activity of the pure silica ITQ2 is negligible compared to to the catalyst containing AgAu nanoclusters supported on the ITQ2 zeolite.

The stability of the catalyst was explored in a long time reaction and by reusability experiments. In the first type of experiments, the reaction temperature was kept constant and the reaction was performed for several hours. The results obtained in a 4 -h reaction at 350 °C with the catalyst pretreated with hydrogen are shown in the Supporting Information (Fig. S4). The CO conversion was around 60 %, this is the same value that was reached in the experiment with the temperature steps at 350 °C (Fig. 1). The activity was constant during the 4 h reaction, with no sign of catalyst deactivation. These results also indicate that these catalysts are appropriate for the treatment of combustion exhaust gases containing CO as they are active in the range 150−500 °C that is the usual temperature of effluent gases in those devices. It must be pointed out the comparison of the catalytic activity of these materials with other gold nanoparticle based catalysts is not feasible as those are mainly used for treatment of indoor gases at low temperature and to the different physical-chemical characteristics of the catalysts used [48,49,60,61].

In the second type of experiments, sequential reactions using the same catalyst sample were performed. The results obtained with the catalyst initially pretreated with oxygen or with hydrogen are shown in Fig. 2. As it can be seen, the catalyst pretreated with hydrogen (left) was highly stable and almost identical results were obtained with this catalyst in the successive runs. This indicates that the metallic active sites formed after this pretreatment in the supported bimetallic nanocluster catalyst were not prone to change. On the other hand, the catalyst pretreated with oxygen (Fig. 2, right) evolved during the reaction and better results were obtained in the second reaction run, indicating that new species were formed. These new species seemed to be more stable since the same catalytic performance was obtained in the third run. It must be pointed out that the catalytic results of the $pretO_2$ supported nanocluster after the second run are the same as those obtained after the

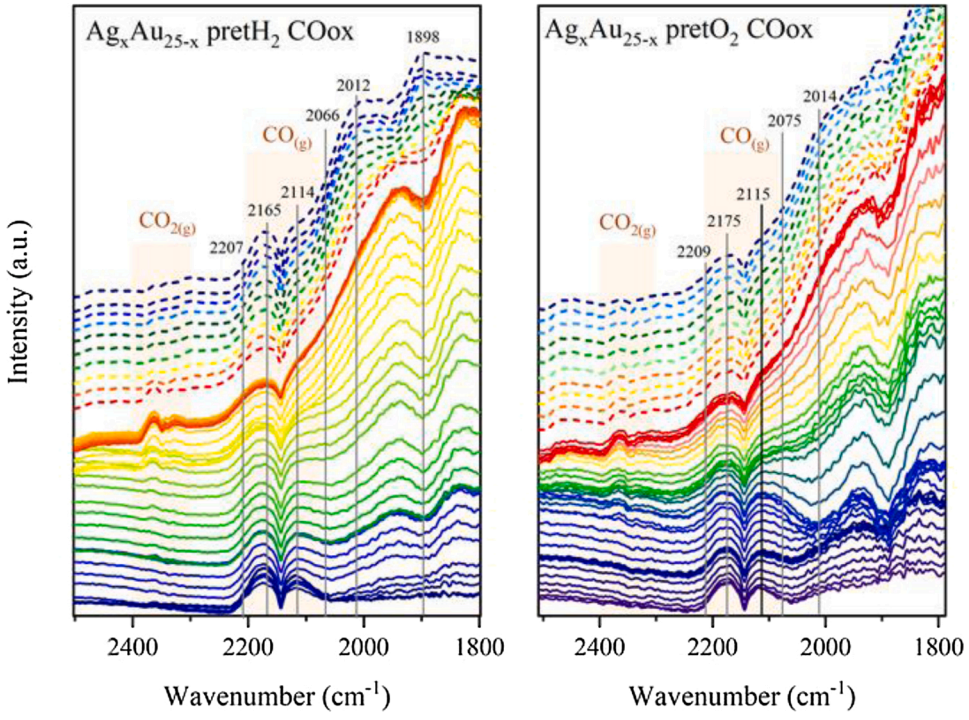

Fig. 4. *In situ* DRIFTS experiment during CO oxidation with the supported bimetallic nanoclusters after different pretreatments ($pretH_2$ and $pretO_2$), from room temperature (blue) to 400 °C (red). Cooling process under reaction conditions from 400 °C (▬) to room temperature (——).

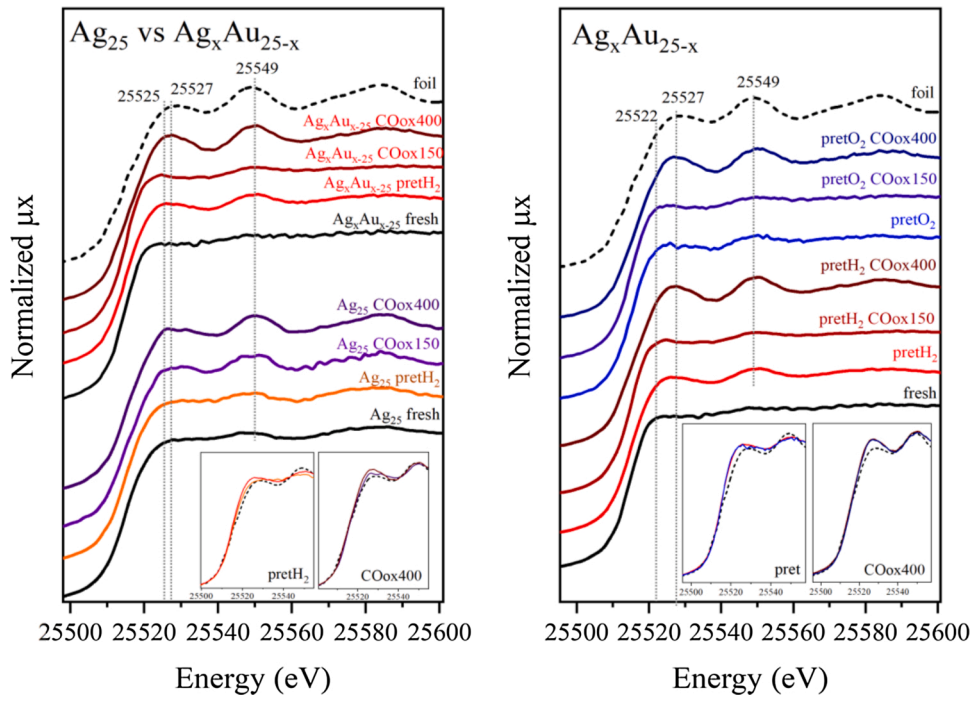

Fig. 5. Normalized XANES spectra at Ag K-edge of Ag_{25}/ITQ2 and Ag_xAu_{25-x}/ITQ2 after H_2 pretreatment and in CO oxidation (left); XANES spectra at Ag K-edge of Ag_xAu_{25-x}/ITQ2 after the different pretreatments and in CO oxidation (right).

hydrogen pretreatment. This indicates that similar species were formed in both cases after reaction.

For a better understanding of the catalytic properties of the supported bimetallic nanocluster, its activity was compared with those obtained with the silver and gold monometallic nanoclusters. This comparison was made with the catalysts activated with hydrogen, as better results were obtained with the Ag_xAu_{25-x}/ITQ2 nanocluster with this pretreatment. The results are shown in Fig. 3.

As it can be seen, after hydrogen activation, the best results were obtained with the supported bimetallic AgAu nanocluster catalyst, which showed activity from 200 °C onwards. For the supported Au nanocluster catalyst, activity only set in at 300 °C, which is 100 °C higher than for the bimetallic nanoclusters. Even higher temperatures were required when applying supported Ag nanoclusters, which only showed a significant increase in activity above 400 °C.

These results suggest that a synergetic effect of the Ag-Au active sites exists on the supported bimetallic nanocluster or that different metallic species are formed in this catalyst, which are more active than those formed in the supported monometallic nanoclusters.

3.2. *In situ* DRIFTS studies

To obtain some insights related to the catalytic activity, *in situ* DRIFTS measurements were carried out during CO oxidation with the Ag_xAu_{25-x}/ITQ2 catalysts after both pretreatments ($pretH_2$ and $pretO_2$). The monometallic catalysts (Ag_{25}/ITQ2 and Au_{25}/ITQ2), as well as the zeolite (ITQ2) were also studied as references (Figs. S4 and S5). Fig. 4 shows the evolution of the infrared spectra from room temperature to 400 °C under reaction conditions, using the bimetallic Ag_xAu_{25-x}/ITQ2 catalyst with different pretreatments.

The on-set of catalytic activity is indicated by the formation of CO_2 gas phase bands (2400−2300 cm^{-1}), which become more pronounced at higher temperatures. Simultaneously, the band related to CO gas phase (2200−2100 cm^{-1}) decreased. In the same region, the possible bands associated with stretching vibrations of CO on gold [13,25] and on silver [62–65] are located complicating the detailed assignment of the bands.

The evolution of the spectra of the differently pretreated catalysts during reaction at increasing temperatures is quite similar. In both cases, at higher temperatures, a shoulder around 2207−2209 cm^{-1} appeared, which stretches over the range of CO-Ag^+ vibrations (around 2160−2190 cm^{-1}) [62–65]. This shoulder could be also related to CO-Au^+ vibrations (around 2175 cm^{-1}) shifted to higher values due to close Ag-Au interaction, which would indicate AgAu alloy particles [64,66], in agreement with the XAFS measurements shown below. The alloying process can be explained because, initially, the Ag atoms were located on the surface of the cluster core, still surrounded by the [S(*R*)-Au]$_2$-S(R) motifs. Increasing the temperature might result in the partial destruction of the ligand shell that favoured the alloying between the two metals, likely enriching Ag on the surface of the AgAu nanoparticles [67–69].

The main difference observed in the spectra of the samples with different pretreatments is the band at around 2070 cm^{-1}, which could be related to CO-Au° [64], and which is much more pronounced for the catalyst pretreated with oxygen, mostly at temperatures of around 250 °C (green spectra in Fig. 4).

The comparison of the spectra of the monometallic catalysts (Fig. S5) with those of the bimetallic nanocluster shows that in the latter, the characteristic bands of CO adsorbed on silver (2160−2190 cm^{-1}) or gold (2120−2110 cm^{-1}) are not clearly observed. Moreover, bands between 1800 and 1970 cm^{-1} appear for all the catalysts. These bands are assigned to carbonates and formates that are formed during the reaction on the support [70] as they also appear in the *in situ* DRIFTS spectra of the ITQ2 zeolite during CO oxidation (Fig. S6).

3.3. *In situ* XAFS studies

The evolution of the nanoclusters supported on the ITQ2 zeolite during pretreatments and in the CO oxidation experiments was followed *in situ* by XAFS. Fig. 5 shows the XANES spectra of the bimetallic Ag_xAu_{25-x} and monometallic Ag_{25} nanoclusters supported on ITQ2 zeolite.

For both, mono and bimetallic catalysts (Fig. 5, left), slightly higher whiteline intensity is observed with the fresh, unpretreated samples in comparison to the Ag foil. In addition, flattening of the oscillations

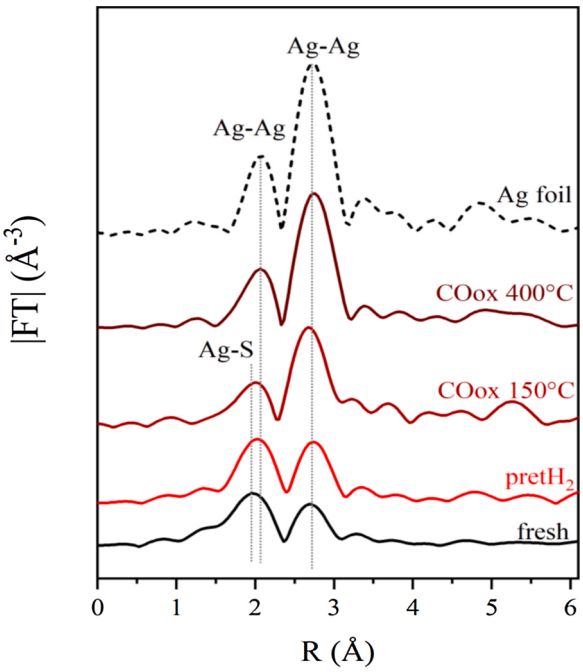

Fig. 6. R space of the Ag_{25}/ITQ2 catalyst: fresh, after H_2 pretreatment and during CO oxidation.

above the edge is denoted, which is in agreement with reported XANES spectra of Ag nanoclusters [31,71,72]. This can be related with the presence of Ag-S bonds, implying partially charged Ag species and leading to a modification in the position and intensity of the whiteline and of other peaks above the edge. It is described that for Ag atoms forming a covalent bond with S, the whiteline systematically shifts to lower energies [72–77].

The comparison of the XANES spectra of the supported mono and bimetallic nanoclusters (Fig. S7) shows the first XAFS evidence on the intimate contact between Ag and Au. The whiteline in the spectrum of the bimetallic sample is shifted towards lower energies in comparison with that of the monometallic one, which can be related to changes in silver electronic configuration when alloyed with gold, according to [71, 78].

The reductive or oxidative pretreatment at 150 °C of the supported bimetallic nanoclusters does not seem to affect the distribution of silver sites in the initial AgAu cluster structure as similar XANES spectra are observed (Fig. 5, right). More pronounced changes are perceived after reaction at 400 °C (_COox400 °C) for both $pretH_2$ and $pretO_2$ bimetallic catalysts. Under these conditions, a shift to higher energy combined with more defined features at around 25,549 eV is noted, showing similarities to the spectrum of Ag foil. This indicates an increase of the metallic character of the clusters over the course of the reaction that can be related to a complete removal of the thiolate ligands (that only occurs at temperatures higher than 150 °C) [13,19] and to the sintering of the metallic species. At this step, the alloying between Ag and Au becomes evident by the presence of shifted oscillations in the χ(k) functions of the catalysts in comparison with metallic silver (Fig. S8), related to the insertion of Au within the Ag metallic structure. These shifts in k-space and antiphase behaviour (see oscillations at ~6 $Å^{-1}$) are a clear indication of metal alloying [79].

More information on the local environment of the nanoclusters and on their structure stability under reaction conditions was obtained from EXAFS analysis. Fig. 6 and Table 1 show the results of the EXAFS fitting for the monometallic Ag_{25}/ITQ2 catalyst (see Fig. S9 for R-space fits). As it can be seen, $pretH_2$ does not lead to significant changes in the Ag_{25}/ITQ2 catalysts (Fig. 6), again confirming the stability of the cluster structure. It can be related to the incomplete removal of the ligands, denoted by the high coordination number (CN) of Ag-S observed in Table 1. However, a complete loss of the ligands occurs under reaction conditions, as is confirmed by the absence of Ag-S bonds in the sample after reaction ($pretH_2$COox400). The reaction led to a change in the CN_{Ag-Ag} from 4.0 to 8.6, but without differences in the previous Ag-Ag bond distance (Table 1).

Fig. 7 and Table 2 show the results of the EXAFS fitting for the bimetallic Ag_xAu_{25-x}/ITQ2 catalyst (see Fig. S9 for R-space fits). In both cases, only Ag-Au and Ag-S bonds are detected after the pretreatment and no signs of Ag-Ag bonds appear, implying dispersion of single Ag atoms across the nanocluster. Besides, the best fitting was obtained by the introduction of Au in the neighbouring of Ag atoms independently of the sample treatment. This is an indication of the formation of Ag-Au alloys in the bimetallic sample.

This metal distribution is modified during the CO oxidation, suggested by the appearance of Ag-Ag bonds (Table 2) and by the disappearance of the Ag-S bonds. Both catalysts after reaction (_COox400 °C) displayed quite a similar surface configuration with almost identical values for CN_{Ag-Au} and bond distances. Thus, the reaction induced a similar evolution of the atomic distribution of the bimetallic nanoclusters, leading to the formation of AuAg nanoparticles that also possess Ag-Ag sites.

3.4. NAP-XPS studies

Further characterization of the bimetallic catalysts was performed by NAP-XPS. The results obtained (Fig. 8) confirm the alloying evolution observed by XAFS studies. The analysis of the AgAu/ITQ catalysts after pretreatment, reveals a peak for Ag $3d_{5/2}$ at 371.8 eV and a peak for Au $4f_{7/2}$ at 87.3 eV, respectively. The first one can be attributed to Ag atoms in the gold clusters. The relatively high binding energy (BE) of this signal could be related with a partial charge transfer from Au to Ag and in the formation of well-defined atomic scale nanoclusters [80,81] that result in higher binding energies. The higher BE observed for the gold signal is caused by a size effect [82] as smaller clusters leads to higher binding energies. The ratio between Au and Ag was calculated based on the peak areas (same cross-section for both elements) obtaining a Au/Ag ratio of 2.4.

After catalytic reaction some changes could be observed by XPS. First, the Ag 3d signal is shifted to lower binding energies (from 371.8 to 370.1 eV), while the Au 4f signal only is shifted 0.1 eV. Furthermore, the ratio between Au and Ag changed to 1.3. This is also observable in the NAP-XPS spectra with a relative increase of the Ag signal and a relative

Table 1
Summary of optimized parameters by fitting the EXAFS data of the Ag_{25}/ITQ2 catalyst.

Sample	Path	CN	R (Å)	σ^2 ($Å^2$)	ΔE_0 (eV)	R_{factor}
Ag foil	Ag-Ag	12	2.862 ± 0.004	0.0096 ± 0.0006	1.9 ± 0.4	0.0036
$pretH_2$[a]	Ag-S	1.7 ± 0.3	2.491 ± 0.023	0.0101 ± 0.0023	3.1 ± 1.6	0.0262
	Ag-Ag	4.0 ± 0.8	2.876 ± 0.017			
$pretH_2$ COox400[b]	Ag-Ag	8.6 ± 0.4	2.861 ± 0.004	0.0093 ± 0.0007	2.6 ± 0.4	0.0020

[a] ΔR = 1.5–3.2 Å over FT of the k^2-weighted χ(k) functions performed in the Δk = 2.0-10.0 $Å^{-1}$ interval.
[b] ΔR = 1.8–3.2 Å over FT of the k^2-weighted χ(k) functions performed in the Δk = 2.0-9.0 $Å^{-1}$ interval. All spectra were collected at ambient temperature (RT-40 °C), except for the samples named CoOx150 which were collected at 150 °C, which, consequently, resulted in higher σ^2 values. $S_0^2 = 0.8$ from Ag metal.

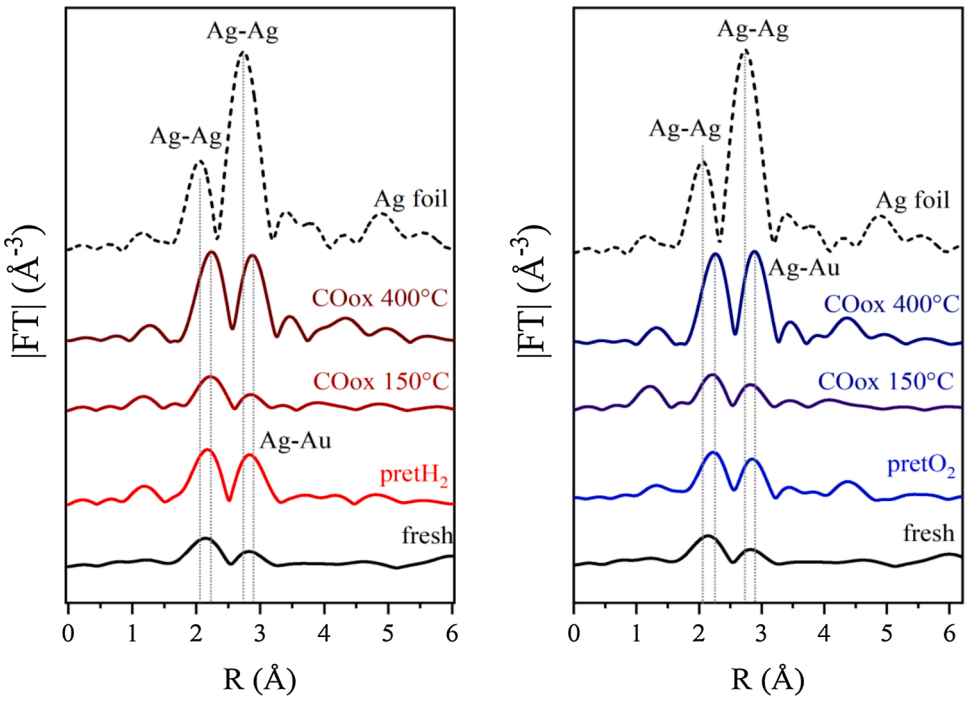

Fig. 7. R space of the Ag_xAu_{25-x}/ITQ2 catalyst: fresh, after the different pretreatments and during CO oxidation ($pretH_2$ on the left and $pretO_2$ on the right).

Table 2
Summary of optimized parameters by fitting the EXAFS data of the AgAu/ITQ2 catalyst.[a].

Sample	Path	CN	R (Å)	σ^2 (Å^2)	ΔE_0 (eV)	R_{factor}
Ag foil	Ag-Ag	12	2.862 ± 0.004	0.0096 ± 0.0006	1.9 ± 0.4	0.0036
$pretO_2$	Ag-S	0.6 ± 0.4	2.570 ± 0.075	0.0094[b]	−0.7 ± 2.1	0.0421
	Ag-Au	5.0 ± 0.9	2.800 ± 0.023			
$pretO_2$ COox400	Ag-Ag	2.0 ± 0.3	2.868 ± 0.025	0.0107 ± 0.0074	2.5 ± 0.6	0.0060
	Ag-Au	7.1 ± 0.7	2.858 ± 0.008			
$pretH_2$	Ag-S	0.9 ± 0.4	2.545 ± 0.046	0.0094[b]	−1.3 ± 2.2	0.0644
	Ag-Au	5.6 ± 0.9	2.786 ± 0.020			
$pretH_2$ COox400	Ag-Ag	2.1 ± 0.3	2.864 ± 0.022	0.0090 ± 0.0017	2.1 ± 0.5	0.0037
	Ag-Au	7.2 ± 0.7	2.858 ± 0.008			

[a] ΔR = 1.6–3.2 Å over FT of the k^2-weighted χ(k) functions performed in the Δk = 2.0-10.0 Å^{-1} interval. All spectra were collected at ambient temperature (RT-40 °C). $S_0^2 = 0.8$ from Ag metal.
[b] The σ^2 was fixed to be the same for the pretreated samples, which decreases the values in error bars.

decrease of the Au signal. These results indicate a migration of silver towards the surface of the catalyst and/or a partial change of the Ag charge [80]. Nevertheless a full oxidation of the Ag atoms can rather be excluded as this would led to different binding energies.

3.5. TEM studies

Morphological changes and composition were studied by TEM-EDX and STEM-HAADF for the AgAu/ITQ2 fresh catalyst and for the same catalyst after the CO oxidation reaction with each of the previous pretreatments (Fig. 9). In the case of the fresh catalysts, particles with 1.5 ± 0.3 nm size were observed. The particles slightly increase their size to 1.7−2 ± 0.5 nm after the CO oxidation reaction. The results show a very homogeneous particle size distribution that is shifted to smaller sizes than in previous works where the nanoparticles have been deposited on mesoporous supports [61]. Similar studies were made with the monometallic Au/ITQ2, observing that the particle size of the fresh catalyst was 1.6 ± 0.4 nm. After the CO oxidation reaction, an increase of the particle size was observed from 1.6 to 2.7 ± 0.5 nm (Fig. S10). EDX analysis of the bimetallic nanoclusters was also performed (Fig. S11), focusing the beam on a particle and observing that there was no segregation of the metals. These results clearly indicate the formation of nanoclusters with a homogeneous alloy.

4. Discussion

The main catalytic results obtained were: i) the higher activity of the bimetallic nanoclusters supported on the zeolite compared to the supported monometallic nanoclusters (Fig. 3), ii) the different activity obtained with the supported AgAu nanoclusters depending on the pretreatment (Fig. 1) and iii) the stability and activity of this catalyst in the successive catalytic runs (Fig. 2).

The catalytic performance can be explained by the characterization studies. As previously discussed, *in situ* DRIFTS experiments suggested that the CO adsorption sites of the bimetallic catalyst are different from those of the monometallic nanoclusters, indicating that Ag-Au alloyed nanoparticles are formed. This was fully confirmed by EXAFS, which shows the presence of Ag-Au bonds in the pretreated samples.

TPR results also corroborate the interaction between Ag and Au in the bimetallic nanoclusters. The TPR patterns of the fresh samples are shown in Supporting Information (Fig. S12), the hydrogen consumption of Au-containing catalysts was much lower than that of Ag-catalyst, indicating that most of the metallic species in Au- and AuAg catalysts were in their reduced state. The opposite occurred to ITQ2 supported Ag

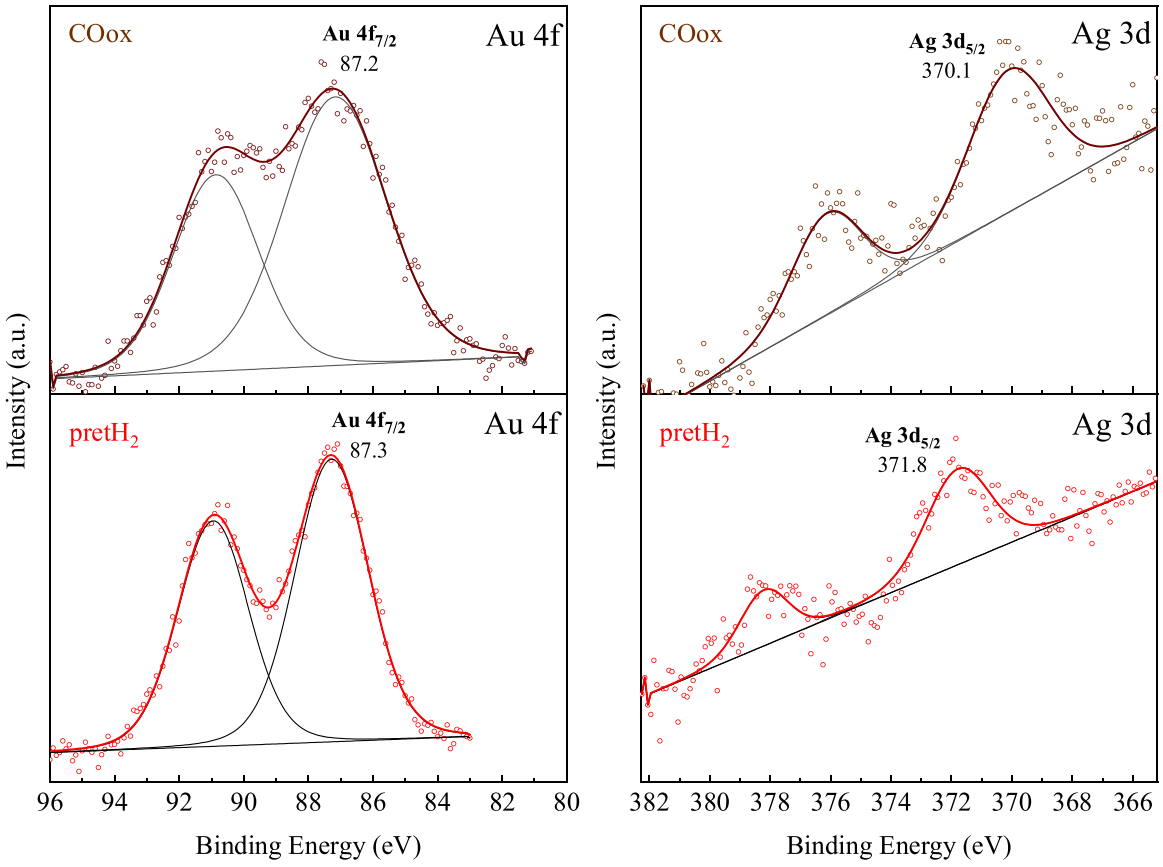

Fig. 8. NAP-XPS spectra of Ag_xAu_{25-x}/ITQ2 catalysts: after pretreatment with H_2 (bottom) and CO oxidation (top).

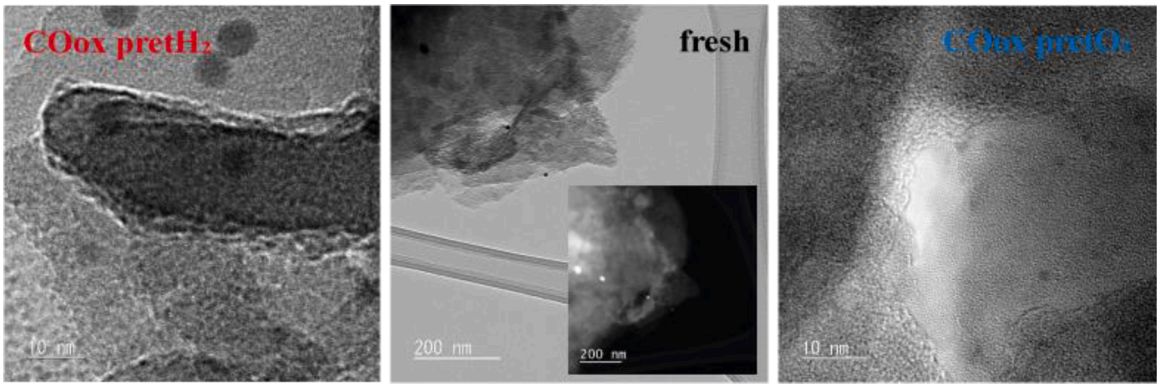

Fig. 9. TEM micrographs of Ag_xAu_{25-x}/ITQ2 catalysts: fresh (middle) and after CO oxidation (right: previous O_2 pretreatment, left: previous H_2 pretretament).

nanoclusters, which were partially oxidized, being reduced at temperatures close to 400 °C. A more detailed analysis of the TPR profiles showed that Au/ITQ2 had a very weak reduction feature at 510 °C, whilst Ag/ITQ2 had a reduction peak at 390 °C. The AgAu cluster supported on ITQ2 featured weak TPR peaks at 310 °C and 528 °C. The high temperature reduction peak arose at similar temperature than the peak in the Au/ITQ2 profile, but the peak at 310 °C appeared clearly at lower temperatures than that observed for Ag/ITQ2. This indicates that Ag reduction was modified by the presence of Au in the bimetallic nanoclusters.

XPS and TEM-EDX studies also showed the formation of homogeneous Ag-Au alloy but no encapsulation of the nanoclusters. Furthermore, no evidence for the formation of Ag-oxide was found with NAP-XPS, therefore we discard the formation of the metal-oxide interface in our catalysts as it was suggested by other authors [83–85]. Nevertheless, we cannot exclude that synergistic effects of the zeolite support and the nanoclusters appear favouring the catalytic activity, as it occurs in other metal containing ITQ2 catalysts used for other reactions [86].

The Ag-Au sites are preferential adsorption sites for CO and O_2 [49] and this results in a higher activity of the bimetallic catalyst compared to the monometallic nanoclusters supported on the ITQ2 zeolite.

The two types of pretreatment were affecting the structure evolution of the supported bimetallic nanocluster, which was reflected in the different catalytic activity. A different arrangement of the Ag atoms within the bimetallic cluster, depending on the pretreatment, can be expected. It was reported that reducing atmosphere induced the migration of Ag mainly to the surface of alloy particles, which was not taking place under oxidative conditions [49]. This results in a higher number of Ag-Au sites on the cluster surface, as observed in the XPS

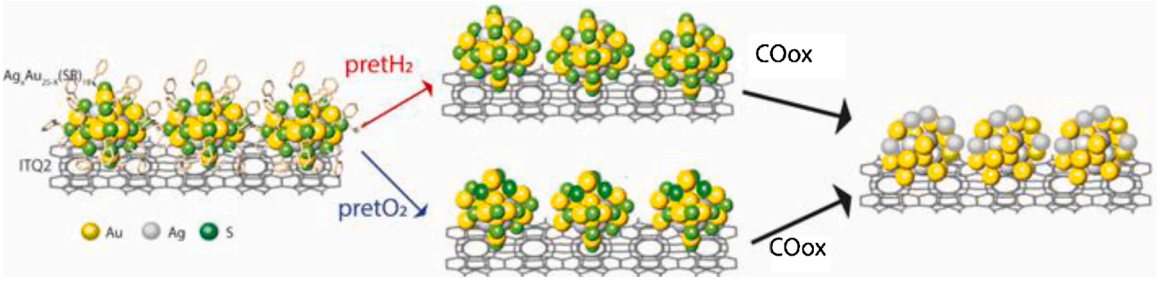

Fig. 10. Changes in the nanocluster structure during pretreatments and reaction.

study, which would be available for reaction (see Fig. 10). Previous studies showed that CO and O_2 co-adsorption on neighbouring sites of the AgAu alloy was stronger than on either Au or Ag [49,50]. Therefore, a larger number of accessible bimetallic sites, formed in a reductive treatment, should enhance the catalytic activity. This explanation is consistent with the catalytic results obtained at lower temperatures showing a higher activity of the sample pretreatment with H_2 compared with that pretreated with oxygen. *In situ* DRIFTS experiments confirmed this postulate as they showed that the bimetallic nanoclusters pretreated with oxygen form CO-Au° adsorbates at medium reaction temperature (250 °C). This proves the presence of monometallic gold sites at this temperature that were not observed for the sample pretreated with hydrogen. The presence of these species suggests that in these conditions (low temperature and oxidative pretreatment) less AgAu nanoparticles are formed leading to lower activity.

Regarding the catalyst stability in successive reactions, it was observed that the catalytic performance of the supported bimetallic nanoparticle pretreated with hydrogen was the same over three runs. However, the catalyst pretreated with oxygen got more active after the first reaction, obtaining in the second run the same catalytic results that those obtained with the catalyst just pretreated with hydrogen. The catalytic performance did not change in a third consecutive reaction. These results are fully consistent with the EXAFS characterization of the different pretreated catalysts after reaction (pretH_2COox400 and pretO_2COox400). Table 2 displays that the same Ag-Au coordination numbers (7.1 and 7.2) were obtained after CO oxidation for both samples even though a different pretreatment was applied. This indicates a dynamic evolution of the catalyst during the reaction that results in the complete removal of the ligands together with the formation of accessible AgAu nanoparticles, in both cases (see Fig. 10).

The EXAFS analysis has also shown that some Ag-Ag sites were formed after reaction with both catalysts subjected to different pretreatments. This was further confirmed by the NAP-XPS results, observing a higher ratio of Ag atoms on surface without segregation or oxidation and verified by the TEM-EDX analysis. Despite that, similar catalytic results were obtained with the reused catalysts compared to the AgAu nanoclusters pretreated with hydrogen, for which no Ag-Ag bonds were observed by EXAFS. Moreover, the activity of the bimetallic catalysts was significantly higher than the one of the Ag_{25} catalyst (which only has silver sites). This suggests that the monometallic centres are not as active as the bimetallic alloy sites, but complementary studies are required to clarify the further evolution of the catalyst surface.

5. Conclusions

Ag doping in Au nanoclusters supported on ITQ2 zeolite leads to the formation of bimetallic AgAu sites which show higher catalytic activity for CO oxidation in comparison to the monometallic centres. These sites are formed by a rearrangement of the metal atoms during pretreatment and reaction. It is observed that a reductive pretreatment initially produces a higher degree of Ag-Au alloying than an oxidative activation. This, in turn, could facilitate the co-adsorption of CO and O_2, which would explain the higher activity observed at lower temperatures for the catalyst pretreated with H_2. Despite these initial differences, during CO oxidation, the differently pretreated bimetallic clusters equally evolve and form similar species after reaction. These species are highly active Ag-Au alloyed nanoparticles and less active Ag-Ag sites. The same catalytic performance is obtained in subsequent catalytic runs independently of the initial pretreatment indicating that the newly formed sites are stable preventing catalyst deactivation.

Within this work, evolution of bimetallic AgAu nanoclusters supported on zeolites during CO oxidation has been disclosed by *in situ* XAFS and DRIFTS studies. These studies provide insight into the mobile nature of bimetallic nanocluster catalysts during reaction, which is a fundamental aspect to be considered in the design of active catalysts for future applications.

CRediT authorship contribution statement

I. López-Hernández: Methodology, Investigation, Data Analysis **V. Truttmann**: Investigation, Data Analysis, **C. Garcia**: Investigation, **C. W. Lopes:** Investigation, **C. Rameshan:** Investigation**, M. Stöger-Pollach:** Investigation, **N. Barrabés:** Original draft preparation, Writing-Reviewing and Editing, Supervision, **G. Rupprechter:** Supervision, Resources **, F. Rey:** Supervision, Reviewing, Resources **A. E. Palomares:** Original draft preparation, Writing- Reviewing and Editing, Supervision.

Declaration of Competing Interest

The authors declare no conflict of interest.

Acknowledgements

The authors thank the Spanish Ministry of Economy and Competitiveness through RTI2018-101784-B-I00 (MINECO/FEDER) and SEV-2016-0683 projects for the financial support. I. López Hernández is grateful to Generalitat Valenciana and European Social Fund for the pre doctoral grant ACIF2017. C.W.L. thanks PRH 50.1 – ANP/FINEP Human Resources Program (Brazil) for the Visiting Researcher Fellowship. We gratefully acknowledge ALBA synchrotron for allocating beamtime (proposal 2015091414) and the CLÆSS beamline staff for their help and technical support during our experiment. We acknowledge support by the Austrian Science Fund (FWF) *via* grants DK+Solids4Fun (W1243), Single Atom Catalysis (I 4434-N) and Elise Richter (V831-N).

Appendix A. Supplementary data

Supplementary material related to this article can be found, in the online version, at doi:https://doi.org/10.1016/j.cattod.2021.04.016.

References

[1] L. Liu, A. Corma, Metal catalysts for heterogeneous catalysis: from single atoms to nanoclusters and nanoparticles, Chem. Rev. 118 (2018) 4981–5079, https://doi.org/10.1021/acs.chemrev.7b00776.
[2] X.Y. Dong, Z.W. Gao, K.F. Yang, W.Q. Zhang, L.W. Xu, Nanosilver as a new generation of silver catalysts in organic transformations for efficient synthesis of

fine chemicals, Catal. Sci. Technol. 5 (2015) 2554–2574, https://doi.org/10.1039/c5cy00285k.
[3] Y. Du, H. Sheng, D. Astruc, M. Zhu, Atomically precise noble metal nanoclusters as efficient catalysts: a bridge between structure and properties, Chem. Rev. 120 (2020) 526–622, https://doi.org/10.1021/acs.chemrev.8b00726.
[4] J. Zhao, R. Jin, Heterogeneous catalysis by gold and gold-based bimetal nanoclusters, Nano Today 18 (2018) 86–102, https://doi.org/10.1016/j.nantod.2017.12.009.
[5] X. Huang, M.A. El-Sayed, Gold nanoparticles: optical properties and implementations in cancer diagnosis and photothermal therapy, J. Adv. Res. 1 (2010) 13–28, https://doi.org/10.1016/j.jare.2010.02.002.
[6] M. Sankar, Q. He, R.V. Engel, M.A. Sainna, A.J. Logsdail, A. Roldan, D.J. Willock, N. Agarwal, C.J. Kiely, G.J. Hutchings, Role of the support in gold-containing nanoparticles as heterogeneous catalysts, Chem. Rev. 120 (2020) 3890–3938, https://doi.org/10.1021/acs.chemrev.9b00662.
[7] T. Ishida, T. Murayama, A. Taketoshi, M. Haruta, Importance of size and contact structure of gold nanoparticles for the genesis of unique catalytic processes, Chem. Rev. 120 (2020) 464–525, https://doi.org/10.1021/acs.chemrev.9b00551.
[8] M. Stratakis, H. Garcia, Catalysis by supported gold nanoparticles: beyond aerobic oxidative processes, Chem. Rev. 112 (2012) 4469–4506, https://doi.org/10.1021/cr3000785.
[9] M. Haruta, T. Kobayashi, H. Sano, N. Yamada, Novel gold catalysts for the oxidation of Carbon Monoxide at a temperature far below 0 °C, Chem. Lett. 16 (1987) 405–408, https://doi.org/10.1246/cl.1987.405.
[10] M. Lamoth, M. Plodinec, L. Scharfenberg, S. Wrabetz, F. Girgsdies, T. Jones, F. Rosowski, R. Horn, R. Schlögl, E. Frei, Supported Ag nanoparticles and clusters for CO oxidation: size effects and influence of the silver-oxygen interactions, ACS Appl. Nano Mater. 2 (2019) 2909–2920, https://doi.org/10.1021/acsanm.9b00344.
[11] B. Qiao, J. Lin, A. Wang, Y. Chen, T. Zhang, J. Liu, Highly active Au1/Co3O4 single-atom catalyst for CO oxidation at room temperature, Cuihua Xuebao Chin. J. Catal. 36 (2015) 1505–1511, https://doi.org/10.1016/S1872-2067(15)60889-0.
[12] B. Zhang, C. García, A. Sels, G. Salassa, C. Rameshan, J. Llorca, K. Hradil, G. Rupprechter, N. Barrabés, T. Bürgi, Ligand and support effects on the reactivity and stability of Au38(SR)24 catalysts in oxidation reactions, Catal. Commun. 130 (2019), 105768, https://doi.org/10.1016/j.catcom.2019.105768.
[13] S. Pollitt, V. Truttmann, T. Haunold, C. Garcia, W. Olszewski, J. Llorca, N. Barrabés, G. Rupprechter, The dynamic structure of Au38(SR)24Nanoclusters supported on CeO2upon pretreatment and CO oxidation, ACS Catal. 10 (2020) 6144–6148, https://doi.org/10.1021/acscatal.0c01621.
[14] Y. Zhu, H. Qian, R. Jin, Catalysis opportunities of atomically precise gold nanoclusters, J. Mater. Chem. 21 (2011) 6793–6799, https://doi.org/10.1039/c1jm10082c.
[15] C. Schilling, M. Ziemba, C. Hess, M.V. Ganduglia-Pirovano, Identification of single-atom active sites in CO oxidation over oxide-supported Au catalysts, J. Catal. 383 (2020) 264–272, https://doi.org/10.1016/j.jcat.2020.01.022.
[16] A.N. Pestryakov, N. Bogdanchikova, A. Simakov, I. Tuzovskaya, F. Jentoft, M. Farias, A. Díaz, Catalytically active gold clusters and nanoparticles for CO oxidation, Surf. Sci. 601 (2007) 3792–3795, https://doi.org/10.1016/j.susc.2007.04.012.
[17] S. Lee, C. Fan, T. Wu, S.L. Anderson, CO oxidation on Aun/TiO2 catalysts produced by size-selected cluster deposition, J. Am. Chem. Soc. 126 (2004) 5682–5683, https://doi.org/10.1021/ja049436v.
[18] Y. Zhu, H. Qian, R. Jin, An atomic-level strategy for unraveling gold nanocatalysis from the perspective of Aun(SR)m nanoclusters, Chem. A Eur. J. 16 (2010) 11455–11462, https://doi.org/10.1002/chem.201001086.
[19] C. García, S. Pollitt, M. van der Linden, V. Truttmann, C. Rameshan, R. Rameshan, E. Pittenauer, G. Allmaier, P. Kregsamer, M. Stöger-Pollach, N. Barrabés, G. Rupprechter, Support effect on the reactivity and stability of Au25(SR)18 and Au144(SR)60 nanoclusters in liquid phase cyclohexane oxidation, Catal. Today 336 (2019) 174–185, https://doi.org/10.1016/j.cattod.2018.12.013.
[20] Y. Li, Y. Chen, S.D. House, S. Zhao, Z. Wahab, J.C. Yang, R. Jin, Interface engineering of gold nanoclusters for CO oxidation catalysis, ACS Appl. Mater. Interfaces. 10 (2018) 29425–29434, https://doi.org/10.1021/acsami.8b07552.
[21] Y. Liu, H. Tsunoyama, T. Akita, S. Xie, T. Tsukuda, Aerobic oxidation of cyclohexane catalyzed by size-controlled au clusters on hydroxyapatite: size effect in the sub-2 nm regime, ACS Catal. 1 (2011) 2–6, https://doi.org/10.1021/cs100043j.
[22] B. Zhang, S. Kaziz, H. Li, M.G. Hevia, D. Wodka, C. Mazet, T. Bürgi, N. Barrabés, Modulation of active sites in supported Au38(SC2H4Ph)24 cluster catalysts: effect of atmosphere and support material, J. Phys. Chem. C. 119 (2015) 11193–11199, https://doi.org/10.1021/jp512022v.
[23] A. Simakov, I. Tuzovskaya, A. Pestryakov, N. Bogdanchikova, V. Gurin, M. Avalos, M.H. Farías, On the nature of active gold species in zeolites in CO oxidation, Appl. Catal. A Gen. 331 (2007) 121–128, https://doi.org/10.1016/j.apcata.2007.07.039.
[24] M. Comotti, W.C. Li, B. Spliethoff, F. Schüth, Support effect in high activity gold catalysts for CO oxidation, J. Am. Chem. Soc. 128 (2006) 917–924, https://doi.org/10.1021/ja0561441.
[25] C. Garcia, V. Truttmann, I. Lopez, T. Haunold, C. Marini, C. Rameshan, E. Pittenauer, P. Kregsamer, K. Dobrezberger, M. Sto, N. Barrabe, G. Rupprechter, Dynamics of Pd Dopant Atoms Inside Au Nanoclusters During Catalytic CO Oxidation, 2020, https://doi.org/10.1021/acs.jpcc.0c05735.
[26] B. Zhang, A. Sels, G. Salassa, S. Pollitt, V. Truttmann, C. Rameshan, J. Llorca, W. Olszewski, G. Rupprechter, T. Bürgi, N. Barrabés, Ligand migration from cluster to support: a crucial factor for catalysis by thiolate-protected gold clusters, Chem. Cat. Chem. 10 (2018) 5372–5376, https://doi.org/10.1002/cctc.201801474.
[27] B. Liu, Z. Liao, X. Xiao, S. Gan, R. Luo, Y. Wu, H. Chen, Y. Fang, J. Dong, Fine-tuned hierarchical architecture of MWW zeolites for highly efficient alkylation via suitable accommodation, Ind. Eng. Chem. Res. 59 (2020) 13932–13939, https://doi.org/10.1021/acs.iecr.0c02409.
[28] A. Palčić, V.V. Ordomsky, Z. Qin, V. Georgieva, V. Valtchev, Tuning zeolite properties for a highly efficient synthesis of propylene from methanol, Chem. A Eur. J. 24 (2018) 13136–13149, https://doi.org/10.1002/chem.201803136.
[29] Y. Lv, X. Wang, D. Gao, X. Ma, S. Li, Y. Wang, G. Song, A. Duan, G. Chen, Hierarchically porous ZSM-5/SBA-15 zeolite: tuning pore structure and acidity for enhanced hydro-upgrading of FCC gasoline, Ind. Eng. Chem. Res. 57 (2018) 14031–14043, https://doi.org/10.1021/acs.iecr.8b02952.
[30] J. Sánchez-Laínez, A. Veiga, B. Zornoza, S.R.G. Balestra, S. Hamad, A.R. Ruiz-Salvador, S. Calero, C. Téllez, J. Coronas, Tuning the separation properties of zeolitic imidazolate framework core-shell structures: via post-synthetic modification, J. Mater. Chem. A. 5 (2017) 25601–25608, https://doi.org/10.1039/c7ta08778k.
[31] I. López-Hernández, C. García, V. Truttmann, S. Pollitt, N. Barrabés, G. Rupprechter, F. Rey, A.E. Palomares, Evaluation of the silver species nature in Ag-ITQ2 zeolites by the CO oxidation reaction, Catal. Today 345 (2020) 22–26, https://doi.org/10.1016/j.cattod.2019.12.001.
[32] A. Ghosh, O.F. Mohammed, O.M. Bakr, Atomic-level doping of metal clusters, Acc. Chem. Res. 51 (2018) 3094–3103, https://doi.org/10.1021/acs.accounts.8b00412.
[33] D.E. Jiang, S. Dai, From superatomic Au 25(SR) 18- to superatomic M@Au 24(SR) 18q core-shell clusters, Inorg. Chem. 48 (2009) 2720–2722, https://doi.org/10.1021/ic8024588.
[34] S. Yamazoe, W. Kurashige, K. Nobusada, Y. Negishi, T. Tsukuda, Preferential location of coinage metal dopants (M = Ag or Cu) in [Au25- xMx(SC2H4Ph)18]- (x ~ 1) as determined by extended X-ray absorption fine structure and density functional theory calculations, J. Phys. Chem. C. 118 (2014) 25284–25290, https://doi.org/10.1021/jp5085372.
[35] P. Lu, X.Y. Kuang, A.J. Mao, Z.H. Wang, Y.R. Zhao, Structural and electronic properties of silver-doped gold clusters Au nAgv ($2 \leq n \leq 10$; V = 0,±1): comparison with pure gold clusters, Mol. Phys. 109 (2011) 2057–2068, https://doi.org/10.1080/00268976.2011.609147.
[36] R. Juarez-Mosqueda, S. Malola, H. Häkkinen, Stability, electronic structure, and optical properties of protected gold-doped silver Ag29-xAux (x = 0-5) nanoclusters, Phys. Chem. Chem. Phys. 19 (2017) 13868–13874, https://doi.org/10.1039/c7cp01440f.
[37] D. Mishra, V. Lobodin, C. Zhang, F. Aldeek, E. Lochner, H. Mattoussi, Gold-doped silver nanoclusters with enhanced photophysical properties, Phys. Chem. Chem. Phys. 20 (2018) 12992–13007, https://doi.org/10.1039/c7cp08682b.
[38] Z. Wang, Z. Zhu, C. Zhao, Q. Yao, X. Li, H. Liu, F. Du, X. Yuan, J. Xie, Silver doping-induced luminescence enhancement and red-shift of gold nanoclusters with aggregation-induced emission, Chem. An Asian J. 14 (2019) 765–769, https://doi.org/10.1002/asia.201801624.
[39] B. Zhang, T. Bürgi, Doping silver increases the Au38(SR)24 cluster surface flexibility, J. Phys. Chem. C. 120 (2016) 4660–4666, https://doi.org/10.1021/acs.jpcc.5b12690.
[40] S. Malola, H. Häkkinen, Chiral inversion of thiolate-protected gold nanoclusters via core reconstruction without breaking a Au-S bond, J. Am. Chem. Soc. 141 (2019) 6006–6012, https://doi.org/10.1021/jacs.9b01204.
[41] R. Jin, K. Nobusada, Doping and alloying in atomically precise gold nanoparticles, Nano Res. 7 (2014) 285–300, https://doi.org/10.1007/s12274-014-0403-5.
[42] J. De Haeck, N. Veldeman, P. Claes, E. Janssens, M. Andersson, P. Lievens, Carbon monoxide adsorption on silver doped gold clusters, J. Phys. Chem. A 115 (2011) 2103–2109, https://doi.org/10.1021/jp111257s.
[43] H.J. Freund, G. Meijer, M. Scheffler, R. Schlögl, M. Wolf, CO oxidation as a prototypical reaction for heterogeneous processes, Angew. Chem. Int. Ed. 50 (2011) 10064–10094, https://doi.org/10.1002/anie.201101378.
[44] Z. Wu, G. Hu, D.E. Jiang, D.R. Mullins, Q.F. Zhang, L.F. Allard, L.S. Wang, S. H. Overbury, Diphosphine-protected Au22 nanoclusters on oxide supports are active for gas-phase catalysis without ligand removal, Nano Lett. 16 (2016) 6560–6567, https://doi.org/10.1021/acs.nanolett.6b03221.
[45] J. Good, P.N. Duchesne, P. Zhang, W. Koshut, M. Zhou, R. Jin, On the functional role of the cerium oxide support in the Au38(SR)24/CeO2 catalyst for CO oxidation, Catal. Today 280 (2017) 239–245, https://doi.org/10.1016/j.cattod.2016.04.016.
[46] X. Nie, H. Qian, Q. Ge, H. Xu, R. Jin, CO oxidation catalyzed by oxide-supported Au 25(SR) 18 nanoclusters and identification of perimeter sites as active centers, ACS Nano 6 (2012) 6014–6022, https://doi.org/10.1021/nn301019f.
[47] Z. Wu, D.E. Jiang, A.K.P. Mann, D.R. Mullins, Z.A. Qiao, L.F. Allard, C. Zeng, R. Jin, S.H. Overbury, Thiolate ligands as a double-edged sword for CO oxidation on CeO 2 supported Au25(SCH2CH2Ph) 18 nanoclusters, J. Am. Chem. Soc. 136 (2014) 6111–6122, https://doi.org/10.1021/ja5018706.
[48] W. Li, C. Liu, H. Abroshan, Q. Ge, X. Yang, H. Xu, G. Li, Catalytic CO oxidation using bimetallic MxAu25-x clusters: a combined experimental and computational study on doping effects, J. Phys. Chem. C. 120 (2016) 10261–10267, https://doi.org/10.1021/acs.jpcc.6b00793.
[49] A.Q. Wang, C.M. Chang, C.Y. Mou, Evolution of catalytic activity of Au-Ag bimetallic nanoparticles on mesoporous support for CO oxidation, J. Phys. Chem. B 109 (2005) 18860–18867, https://doi.org/10.1021/jp051530q.
[50] Y. Chi, L. Zhao, X. Lu, C. An, W. Guo, C.M.L. Wu, Effect of alloying on the stabilities and catalytic properties of Ag–Au bimetallic subnanoclusters: a theoretical investigation, J. Mater. Sci. 51 (2016) 5046–5060, https://doi.org/10.1007/s10853-016-9808-8.

[51] P. Kaminski, I. Sobczak, P. Decyk, M. Ziolek, W.J. Roth, B. Campo, M. Daturi, Zeolite MCM-22 modified with Au and Cu for catalytic total oxidation of methanol and carbon monoxide, J. Phys. Chem. C. 117 (2013) 2147–2159, https://doi.org/10.1021/jp310505y.
[52] M.M. Schubert, S. Hackenberg, A.C. Van Veen, M. Muhler, V. Plzak, J.J. Behm, CO oxidation over supported gold catalysts -"Inert" and "active" support materials and their role for the oxygen supply during reaction, J. Catal. 197 (2001) 113–122, https://doi.org/10.1006/jcat.2000.3069.
[53] M. Gąsior, B. Grzybowska, K. Samson, M. Ruszel, J. Haber, Oxidation of CO and C3 hydrocarbons on gold dispersed on oxide supports, Catal. Today 91–92 (2004) 131–135, https://doi.org/10.1016/j.cattod.2004.03.021.
[54] A. Corma, V. Fornés, J.M. Guil, S. Pergher, T.L.M. Maesen, J.G. Buglass, Preparation, characterisation and catalytic activity of ITQ-2, a delaminated zeolite, Microporous Mesoporous Mater. 38 (2000) 301–309, https://doi.org/10.1016/S1387-1811(00)00149-9.
[55] A. Shivhare, S.J. Ambrose, H. Zhang, R.W. Purves, R.W.J. Scott, Stable and recyclable Au25 clusters for the reduction of 4-nitrophenol, Chem. Commun. 49 (2013) 276–278, https://doi.org/10.1039/c2cc37205c.
[56] C.P. Joshi, M.S. Bootharaju, M.J. Alhilaly, O.M. Bakr, [Ag25(SR)18]-: the "golden"silver nanoparticle silver nanoparticle, J. Am. Chem. Soc. 137 (2015) 11578–11581, https://doi.org/10.1021/jacs.5b07088.
[57] B. Ravel, M. Newville, ATHENA, ARTEMIS, HEPHAESTUS: data analysis for X-ray absorption spectroscopy using IFEFFIT, J. Synchrotron Radiat. 12 (2005) 537–541, https://doi.org/10.1107/S0909049505012719.
[58] J.J. Rehr, R.C. Albers, Theoretical approaches to x-ray absorption fine structure, Rev. Mod. Phys. 72 (2000) 621–654, https://doi.org/10.1103/RevModPhys.72.621.
[59] R. Coloma Ribera, R.W.E. Van De Kruijs, J.M. Sturm, A.E. Yakshin, F. Bijkerk, In vacuo growth studies of Ru thin films on Si, SiN, and SiO2 by high-sensitivity low energy ion scattering, J. Appl. Phys. 120 (2016), https://doi.org/10.1063/1.4960577.
[60] C.W. Yen, M.L. Lin, A. Wang, S.A. Chen, J.M. Chen, C.Y. Mou, CO oxidation catalyzed by Au-Ag bimetallic nanoparticles supported in mesoporous silica, J. Phys. Chem. C. 113 (2009) 17831–17839, https://doi.org/10.1021/jp9037683.
[61] A. Wang, Y.P. Hsieh, Y.F. Chen, C.Y. Mou, Au-Ag alloy nanoparticle as catalyst for CO oxidation: effect of Si/Al ratio of mesoporous support, J. Catal. 237 (2006) 197–206, https://doi.org/10.1016/j.jcat.2005.10.030.
[62] E. Kolobova, A. Pestryakov, A. Shemeryankina, Y. Kotolevich, O. Martynyuk, H. J. Tiznado Vazquez, N. Bogdanchikova, Formation of silver active states in Ag/ZSM-5 catalysts for CO oxidation, Fuel. 138 (2014) 65–71, https://doi.org/10.1016/j.fuel.2014.07.011.
[63] K.I. Hadjiivanov, IR study of CO and NOx sorption on Ag-ZSM-5, Microporous Mesoporous Mater. 24 (1998) 41–49, https://doi.org/10.1016/S1387-1811(98)00147-4.
[64] M. Stucchi, A. Jouve, A. Villa, G. Nagy, M. Németh, C. Evangelisti, R. Zanella, L. Prati, Gold-silver catalysts: ruling factors for establishing synergism, Chem. Cat. Chem. 11 (2019) 4043–4053, https://doi.org/10.1002/cctc.201900591.
[65] Z. Qu, S. Zhou, W. Wu, C. Li, X. Bao, CO adsorption and correlation between CO surface coverage and activity/selectivity of preferential CO oxidation over supported Ag catalyst: an in situ FTIR study, Catal. Letters 101 (2005) 21–26, https://doi.org/10.1007/s10562-004-3742-0.
[66] J. Velasquez, B. Njegic, M.S. Gordon, M.A. Duncan, IR photodissociation spectroscopy and theory of Au+(CO) n complexes: nonclassical carbonyls in the gas phase, J. Phys. Chem. A 112 (2008) 1907–1913, https://doi.org/10.1021/jp711099u.
[67] R. Atwi, A. Tuel, M. Maffre, L. Burel, J.L. Rousset, F. Meunier, Highly dispersed Au, Ag and Au-Ag alloy nanoparticles encapsulated in single crystal multi-hollow silicalite-1, Appl. Catal. A Gen. 569 (2019) 86–92, https://doi.org/10.1016/j.apcata.2018.10.028.
[68] W.R. Tyson, W.A. Miller, Surface free energies of solid metals. Estimation from liquid surface tension measurements, Surf. Sci. 62 (1977) 267–276.
[69] S. Hannemann, J.D. Grunwaldt, F. Krumeich, P. Kappen, A. Baiker, Electron microscopy and EXAFS studies on oxide-supported gold-silver nanoparticles prepared by flame spray pyrolysis, Appl. Surf. Sci. 252 (2006) 7862–7873, https://doi.org/10.1016/j.apsusc.2005.09.065.
[70] K. Okumura, K. Yoshino, K. Kato, M. Niwa, Quick XAFS studies on the Y-type zeolite supported au catalysts for CO-O2 reaction, J. Phys. Chem. B 109 (2005) 12380–12386, https://doi.org/10.1021/jp051021o.
[71] J. Liu, K.S. Krishna, C. Kumara, S. Chattopadhyay, T. Shibata, A. Dass, C.S.S. R. Kumar, Understanding Au∼98Ag∼46(SR)60 nanoclusters through investigation of their electronic and local structure by X-ray absorption fine structure, RSC Adv. 6 (2016) 25368–25374, https://doi.org/10.1039/c5ra27396j.
[72] B. Zhang, O.V. Safonova, S. Pollitt, G. Salassa, A. Sels, R. Kazan, Y. Wang, G. Rupprechter, N. Barrabés, T. Bürgi, On the mechanism of rapid metal exchange between thiolate-protected gold and gold/silver clusters: a time-resolved: in situ XAFS study, Phys. Chem. Chem. Phys. 20 (2018) 5312–5318, https://doi.org/10.1039/c7cp08272j.
[73] N.V. Hudson-Smith, P.L. Clement, R.P. Brown, M.O.P. Krause, J.A. Pedersenc, C. L. Haynes, Research highlights: speciation and transformations of silver released from Ag NPs in three species, Environ. Sci. Technol. 3 (2016) 1236, https://doi.org/10.1021/es7032718.
[74] G. Veronesi, A. Deniaud, T. Gallon, P.H. Jouneau, J. Villanova, P. Delangle, M. Carrière, I. Kieffer, P. Charbonnier, E. Mintz, I. Michaud-Soret, Visualization, quantification and coordination of Ag+ ions released from silver nanoparticles in hepatocytes, Nanoscale. 8 (2016) 17012–17021, https://doi.org/10.1039/c6nr04381j.
[75] G. Veronesi, C. Aude-Garcia, I. Kieffer, T. Gallon, P. Delangle, N. Herlin-Boime, T. Rabilloud, M. Carrière, Exposure-dependent Ag+ release from silver nanoparticles and its complexation in AgS2 sites in primary murine macrophages, Nanoscale. 7 (2015) 7323–7330, https://doi.org/10.1039/c5nr00353a.
[76] R. Kaegi, A. Voegelin, B. Sinnet, S. Zuleeg, H. Hagendorfer, M. Burkhardt, H. Siegrist, Behavior of metallic silver nanoparticles in a pilot wastewater treatment plant, Environ. Sci. Technol. 45 (2011) 3902–3908, https://doi.org/10.1021/es1041892.
[77] C.L. Doolette, M.J. McLaughlin, J.K. Kirby, D.J. Batstone, H.H. Harris, H. Ge, G. Cornelis, Transformation of PVP coated silver nanoparticles in a simulated wastewater treatment process and the effect on microbial communities, Chem. Cent. J. 7 (2013) 1–18, https://doi.org/10.1186/1752-153X-7-46.
[78] E. Bus, J.A. Van Bokhoven, Electronic and geometric structures of supported platinum, gold, and platinum-gold catalysts, J. Phys. Chem. C. 111 (2007) 9761–9768, https://doi.org/10.1021/jp067414k.
[79] A.I. Frenkel, Applications of extended X-ray absorption fine-structure spectroscopy to studies of bimetallic nanoparticle catalysts, Chem. Soc. Rev. 41 (2012) 8163–8178, https://doi.org/10.1039/c2cs35174a.
[80] J.N. O'Shea, J. Schnadt, S. Andersson, L. Patthey, S. Rost, A. Giertz, B. Brena, J. O. Forsell, A. Sandell, O. Björneholm, P.A. Brühwiler, N. Mårtensson, X-ray photoelectron spectroscopy of low surface concentration mass-selected Ag clusters, J. Chem. Phys. 113 (2000) 9233–9238, https://doi.org/10.1063/1.1319700.
[81] T. Chen, S. Yang, J. Chai, Y. Song, J. Fan, B. Rao, H. Sheng, H. Yu, M. Zhu, Crystallization-induced emission enhancement: a novel fluorescent Au-Ag bimetallic nanocluster with precise atomic structure, Sci. Adv. 3 (2017) 1–8, https://doi.org/10.1126/sciadv.1700956.
[82] P. Zhang, X - Ray Spectroscopy of Gold – Thiolate Nanoclusters, 2014.
[83] C.H. Wu, C. Liu, D. Su, H.L. Xin, H.T. Fang, B. Eren, S. Zhang, C.B. Murray, M. B. Salmeron, Bimetallic synergy in cobalt–palladium nanocatalysts for CO oxidation, Nat. Catal. 2 (2019) 78–85, https://doi.org/10.1038/s41929-018-0190-6.
[84] T.S. Kim, J. Kim, H.C. Song, D. Kim, B. Jeong, J. Lee, J.W. Shin, R. Ryoo, J.Y. Park, Catalytic synergy on PtNi bimetal catalysts driven by interfacial intermediate structures, ACS Catal. 10 (2020) 10459–10467, https://doi.org/10.1021/acscatal.0c02467.
[85] J. Kim, W.H. Park, W.H. Doh, S.W. Lee, M.C. Noh, J.J. Gallet, F. Bournel, H. Kondoh, K. Mase, Y. Jung, B.S. Mun, J.Y. Park, Adsorbate-driven reactive interfacial Pt-NiO1−x nanostructure formation on the Pt3Ni(111) alloy surface, Sci. Adv. 4 (2018) 1–8, https://doi.org/10.1126/sciadv.aat3151.
[86] M. Moreno-González, A.E. Palomares, M. Chiesa, M. Boronat, E. Giamello, T. Blasco, Evidence of a Cu^{2+}–alkane interaction in cu-zeolite catalysts crucial for the selective catalytic reduction of NOx with hydrocarbons, ACS Catal. 7 (5) (2017) 3501–3509, https://doi.org/10.1021/acscatal.6b03473.